



Assessing brain state and anesthesia level with two-photon calcium signals

Núria Tort-Colet, Francesco Resta, Elena Montagni, Francesco Pavone, Anna Letizia Allegra Mascaro, Alain Destexhe

► To cite this version:

Núria Tort-Colet, Francesco Resta, Elena Montagni, Francesco Pavone, Anna Letizia Allegra Mascaro, et al.. Assessing brain state and anesthesia level with two-photon calcium signals. Scientific Reports, 2023, 13 (1), pp.3183. 10.1038/s41598-023-30224-8 . hal-04040686

HAL Id: hal-04040686

<https://hal.science/hal-04040686>

Submitted on 22 Mar 2023

HAL is a multi-disciplinary open access archive for the deposit and dissemination of scientific research documents, whether they are published or not. The documents may come from teaching and research institutions in France or abroad, or from public or private research centers.

L'archive ouverte pluridisciplinaire **HAL**, est destinée au dépôt et à la diffusion de documents scientifiques de niveau recherche, publiés ou non, émanant des établissements d'enseignement et de recherche français ou étrangers, des laboratoires publics ou privés.



OPEN

Assessing brain state and anesthesia level with two-photon calcium signals

Núria Tort-Colet^{1✉}, Francesco Resta², Elena Montagni², Francesco Pavone^{2,3,4}, Anna Letizia Allegra Mascaro^{2,5,6} & Alain Destexhe^{1,6✉}

Brain states, such as wake, sleep, or different depths of anesthesia are usually assessed using electrophysiological techniques, such as the local field potential (LFP) or the electroencephalogram (EEG), which are ideal signals for detecting activity patterns such as asynchronous or oscillatory activities. However, it is technically challenging to have these types of measures during calcium imaging recordings such as two-photon or wide-field techniques. Here, using simultaneous two-photon and LFP measurements, we demonstrate that despite the slower dynamics of the calcium signal, there is a high correlation between the LFP and two-photon signals taken from the neuropil outside neuronal somata. Moreover, we find the calcium signal to be systematically delayed from the LFP signal, and we use a model to show that the delay between the two signals is due to the physical distance between the recording sites. These results suggest that calcium signals alone can be used to detect activity patterns such as slow oscillations and ultimately assess the brain state and level of anesthesia.

Anesthesia levels and brain states are classified according to the main features of global dynamics such as the frequency of the slow oscillations or the duration of the Up-state and Down-state^{12,37}. Electrophysiological methods are commonly adopted to categorize brain states and to investigate the features of neural activation underlying a specific brain state over multiple scales. In particular, local field potential (LFP) is used to record both single unit and small population activity nearby the electrode, whereas electrocorticogram (ECoG) and electroencephalogram (EEG) are exploited to study neuronal activity dynamics at a larger scale. However, the electrophysiological recordings are poorly defined in terms of the type and spatial distribution of the cell originating the signal. To record the activity of up to hundreds of neurons simultaneously with cellular and subcellular resolution, Two-photon (2P) fluorescence microscopy is increasingly adopted in neuroscience laboratories²⁸. This technique has been applied to the study of neuronal activity dynamics during sleep and anesthesia^{7,40}. In particular, it has been demonstrated that the calcium activity from the neuropil of the cortical layer 2/3 is highly correlated with the electrical (ECoG) signal¹⁹. This pioneering study took advantage of 2P calcium imaging coupled with the calcium dye OGB-1-AM. Calcium dyes provide unspecific labeling of all types of neurons and astrocytes, thus limiting the possibility of identifying the cellular origin of the recorded optical signal.

To overcome this limitation, population-specific labeling of the neurons by genetically encoded calcium indicators (GECI) is increasingly adopted^{18,30}. For instance, activity recordings of GECI via fiber photometry revealed a cortex-wide BOLD signal correlated with the local slow calcium wave signal^{1,29}. In combination with GECIs, 2P fluorescence microscopy enables visualizing the activity of specific neuronal populations with subcellular resolution. Recent studies in rodents including^{20,31} in brain slices or^{4,39} *in vivo*, compared neuronal activity measured via electrophysiology recordings and 2P calcium imaging of small networks, to characterize the transform between neural activity and calcium-related fluorescence. This combination of techniques can provide valuable insight into how information on the brain state is represented and processed in specific neural circuits^{15,24–27,33}. However, these studies rely on the electrical (electromyographical or EEG) signal as background information to define the brain state. It would be useful for the neuroscience and neuroimaging communities to use the 2P fluorescence signal to define the brain state and not rely on simultaneous electrical registrations, which are technically hard to arrange in most experimental setups. It is very important to combine different

¹Paris-Saclay University, CNRS, Institut des Neurosciences (NeuroPSI), Saclay, France. ²European Laboratory for Non-Linear Spectroscopy (LENs), Sesto Fiorentino, Italy. ³Department of Physics and Astronomy, University of Florence, Sesto Fiorentino, Italy. ⁴National Institute of Optics, National Research Council, Sesto Fiorentino, Italy. ⁵Neuroscience Institute, National Research Council, Pisa, Italy. ⁶These authors contributed equally: Letizia Allegra Mascaro and Alain Destexhe. ✉email: n.tort-colet@cnrs.fr; alain.destexhe@cnrs.fr

measurement methods to validate findings independently of the technique used. However, performing such comparisons is not a trivial task and, so far, only rarely addressed.

Because the neuropil volume is dominated by axons, dendrites, and synapses, and since the LFP is thought to be generated essentially from synaptic currents⁹, we reasoned the neuropil calcium signal from excitatory neurons could provide a good proxy for the LFP *in vivo*. Since the optical signal recorded from specific neuronal populations may reflect the activation of slightly diverse and partially overlapping groups of neurons recorded with the LFP, the effect of anesthesia on those signals could be different, and therefore change their correlations. In addition, the spatial distributions of the neurons generating the two signals are different since the two-photon imaging records the activity from a single plane (with a thickness of a few microns) while the LFP reports the electrical activity originated from cells in a hundred of microns virtual sphere around the electrode, depending on the experimental configuration (e.g. relative distance between the electrode and the reference). This difference might also contribute to brain state-dependent changes in their correlations.

Here we evaluated the extent to which the 2P calcium signal from the neuropil in layer 2/3 could be used to determine the brain state. To this aim, we performed simultaneous *in vivo* two-photon calcium imaging and LFP recordings in layer 2/3 of the somatosensory cortex from Thy1-GCaMP6f mice, which express the calcium indicator GCaMP6f selectively in excitatory neurons¹¹. Exploiting this model, we characterized the correlation of the LFP and calcium signals and evaluated its dependence on the anesthesia level. Also, we assessed how reliable is the 2P calcium signal to detect Up and Down states and assess the brain state via the neuropil signal alone. Finally, simulation of the neuropil 2P calcium and LFP signals with a topological spiking network model of AdEx neurons explored the origin of the brain state-dependent correlations.

Results

Simultaneous electrophysiological recordings and calcium imaging. The local field potential (LFP) and the calcium signal of the somatosensory cortex were recorded simultaneously in $n=8$ Thy1-GCaMP6f mice anesthetized with different concentrations of isoflurane. The two-photon calcium recordings were performed in an area of $600 \times 300 \mu\text{m}^2$ over the primary somatosensory (S1) cortical area, with a resolution of 1024×512 pixels. The LFP signal was obtained with a pipette loaded with 1mM Rhodamine dye placed at the edge of the calcium imaging area at a depth of $254.6 \pm 90.1 \mu\text{m}$ (average across 67 recordings), that is, at the level of the superficial layers (Figure 1).

Measuring the correlation between two-photon and LFP recordings. In order to demonstrate that we can use either the LFP or the calcium signals to assess the brain state we first computed the correlation between the two-photon calcium signal resulting from the average over all the pixels, the Field of View (FOV), and the LFP signal in each recording (Figure 2). At the population level ($n=8$ mice; 67 recordings), LFP and FOV signals were highly correlated: Pearson correlation was 0.48 ± 0.12 on average and the median peak correlation was 0.58 ± 0.12 . Interestingly, the calcium signal was delayed with respect to the LFP signal by 0.13 ± 0.03 seconds on average (Figure 2).

Despite the presence of this delay in all recordings, we observed that the distribution of delay values was not uniform. We hypothesised that different depths of anesthesia, that produce a distinct level of synchronization of the cortical network, could lead to different delays. To check this hypothesis we wanted to classify the recordings by the level of anesthesia at which they were obtained. The different isoflurane doses administered to the mice in order to achieve different levels of anesthesia largely varied across subjects. A more reliable way to determine the level of anesthesia in electrophysiological data consists in computing the length of the Down states or the frequency of the slow oscillation^{12,37}. Therefore, we detected Up and Down states from the LFP signal in each recording and defined three groups of recordings based on the frequency of the slow oscillation (Figure 3). We computed the frequency of the slow oscillation in each recording as the inverse of the sum of the median duration of Up and Down states. According to this classification, the group with faster slow oscillations had 23 recordings, the group of intermediate slow oscillation frequency had 24 recordings and the group with slower slow oscillation frequency had 20 recordings.

After classifying the recordings in three groups of decreasing slow oscillation frequency (which corresponds to deeper anesthesia) we observed that the average correlation between the LFP and the FOV signals did not change with the level of anesthesia. On the contrary, the delay between the LFP and the two-photon signal was significantly smaller for deeper anesthesia (Figure 4). In any case, in the deeper anesthesia group, the median delay was still 100ms, and we wondered if this delay could be originated by the nature of the FOV signal, compared to the nature of the LFP: while the LFP records the synaptic activity, which reflects the “electric input” to the local network, the FOV signal includes both the synaptic activity arriving to the cells and the calcium spikes of the recorded units, reflecting both the “calcium input” and the “calcium output”. To check if the delay could be produced by the time needed for the cells to integrate the inputs and spike, we decided to compute the neuropil (NPL) signal by subtracting the two-photon activity of each individual cell identified in the imaged area from the FOV signal (Figure 1).

Then, we computed the Pearson correlation and the cross-correlation between LFP and NPL signals for each recording, as we had done for the FOV signal (Figure 2). The population averages ($n=8$ mice; 67 recordings) show that LFP and NPL signals were highly correlated as well: Pearson correlation was 0.48 ± 0.12 on average and the median peak correlation was 0.59 ± 0.12 . Again, the NPL calcium signal was delayed with respect to the LFP signal by 0.13 ± 0.03 seconds on average (Figure 5).

Finally, we plotted the values of Pearson's correlation, peak cross-correlation and delay to peak against the level of anesthesia for the NPL signal, using the previous classification of recordings in 3 groups of decreasing slow oscillation frequency. As in the case of the FOV signal, the correlation between the LFP and the NPL signals

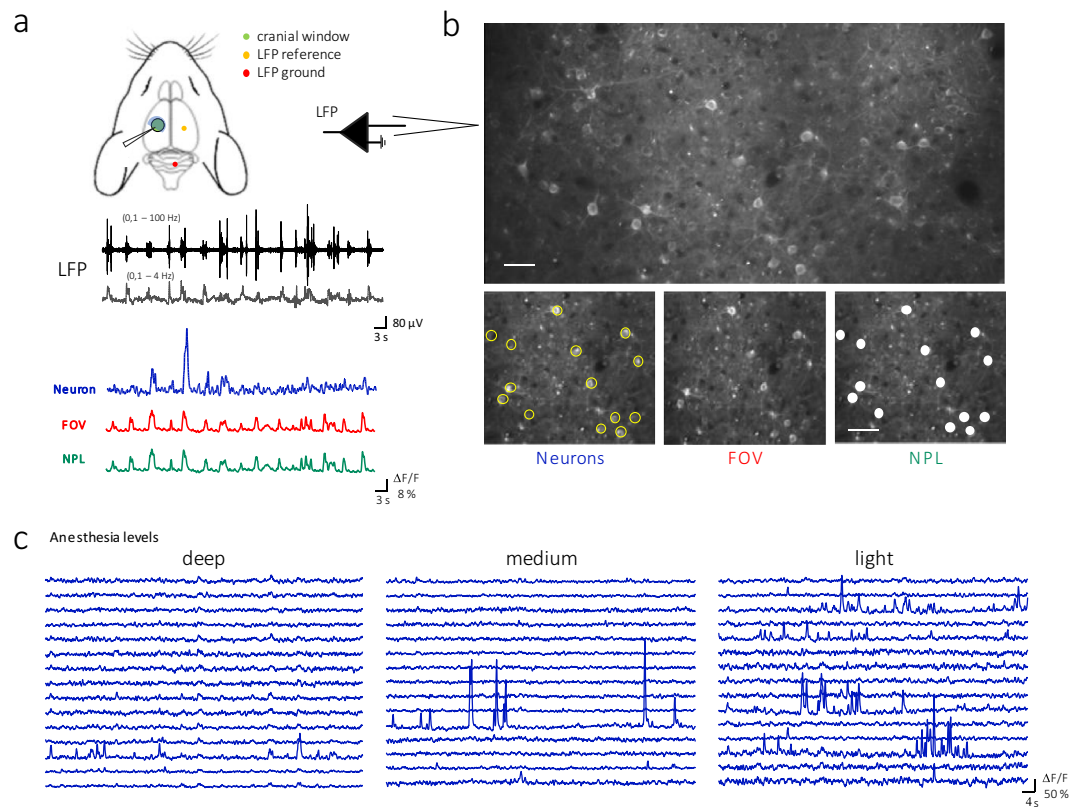


Figure 1. Simultaneous electrophysiological and two-photon imaging recording of L2/3 excitatory neurons activity in GCaMP6f mice. **a. Top.** Experimental scheme. **Bottom.** Representative traces showing the same temporal segment for LFP (black, delta band in grey), Neurons (blue), FOV (red), and NPL (green). **b. Top.** Representative image of two-photon recording of L2/3 excitatory neurons in somatosensory cortex. Scale bar = 30 μm . **Bottom.** Representative ROIs used to extract the calcium dynamics signal from the Neurons (yellow circles), the entire Field Of View (FOV), and the Neuropil (NPL, FOV - Neurons). Scale bar = 45 μm . **c.** Representative time series extracted from 15 neurons in different levels of anesthesia (in this example, corresponding to decreasing percentages of isoflurane concentration).

remained high regardless of the level of anesthesia, and the delay to peak showed a significant reduction towards deeper anesthesia (Figure 5, last row).

Explaining the delay with a topological spiking network model of AdEx neurons. From the results shown, we conclude on one hand, that the FOV signal correlates well with the LFP signal and that this correlation is independent of the brain state. On the other hand, we have observed that the FOV signal is delayed with respect to the LFP signal on average by 130 ms. This delay is not due to the fact that the FOV signal contains cell's activity and the delay is brain state dependent, finding the smallest delays in deep anesthesia.

Since the LFP pipette is inserted *besides* the FOV region, the network recorded by the LFP could be slightly different to the one imaged through the two-photon scanner. We hypothesised that this mismatch in the neuronal populations recorded by each technique would produce a delay between signals, and the smaller delay found at deeper anesthesia levels could be explained by the increased global cortical synchrony induced by the anesthesia⁶.

To evaluate this hypothesis we used a topological spiking network of 10k adaptive exponential integrate and fire (AdEx) neurons⁸ randomly placed in a 2D area of 1700x600 μm with a distance-dependent rule for connectivity (see Methods section). We simulated the spontaneous activity of a cortical network at three different levels of anesthesia by increasing the adaptation strength that affects excitatory neurons only, and that is related to the acetylcholine neuromodulation responsible for the loss of consciousness during sleep or anesthesia^{2,23,37}. Increasing the level of adaptation (from $b = 10\text{pA}$ to 30pA and 60pA) produced slow oscillations with shorter Up states, longer Down states and lower frequency (Figure 6).

In each simulation, we computed the calcium signal from 160 excitatory and 40 inhibitory neurons located within a fixed 600x300 μm area of the network (Figure 7). As in², both the membrane potential and the spikes obtained in the simulations were used to compute the calcium currents, the calcium concentration and finally the calcium fluorescence for each population.

For the LFP computation, we considered all the neurons located at different 600x300 μm areas at increasing distances from the calcium area (see Figure 7C). For each condition (*centered, overlapped, adjacent* and *far* for 0, 300, 600 and 900 μm between the FOV and the LFP areas, respectively), the spikes of each neuron in each

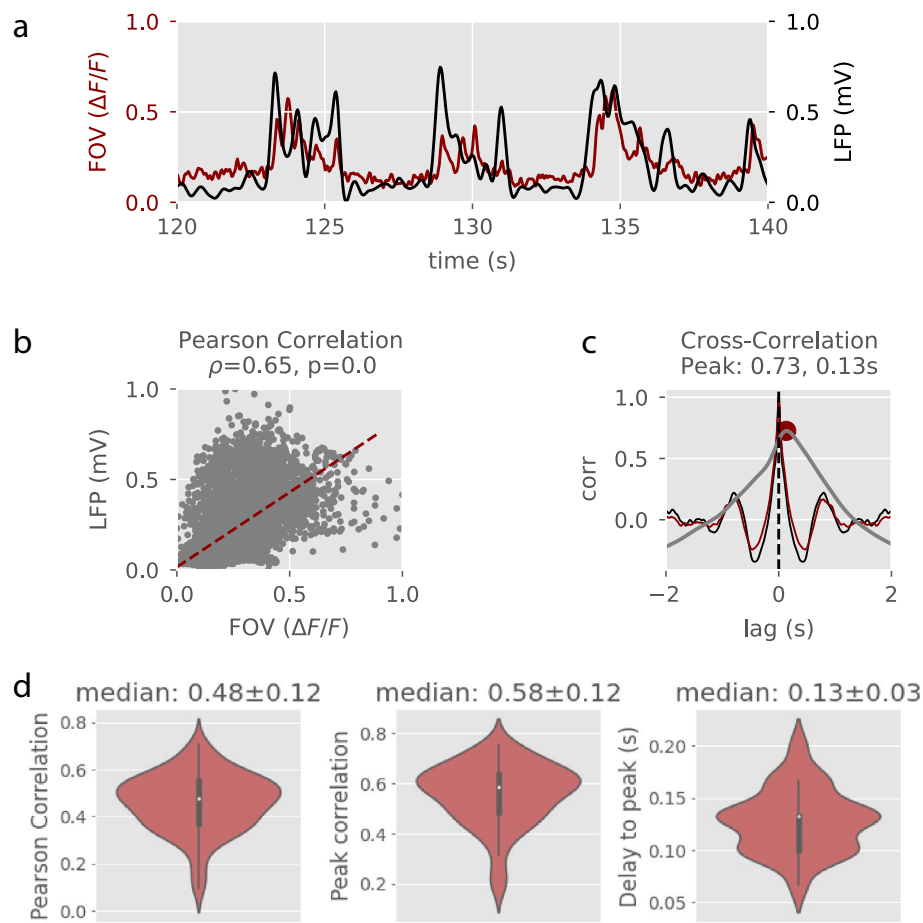


Figure 2. Correlation measures. **a.** Two-photon and LFP normalized signals during 20 seconds of an example recording at 1.5% isoflurane anesthesia. **b.** Pearson's correlation. **c.** Auto- and cross-correlation of LFP (black trace) and FOV (red trace) signals. The cross-correlation (grey trace) peak is depicted with a red dot. **d.** From left to right, median values of the Pearson's correlation, the cross-correlation peak and delay to the cross-correlation peak across $n = 67$ recordings (8 mice).

population were convolved with a kernel to obtain the unitary LFP that would be recorded at the center of the LFP area using the method described in³⁵.

For simplicity, we considered the averaged signal of the excitatory and inhibitory populations, for both the calcium and the LFP signals. We then computed the Pearson's correlation and the cross-correlation between the two signals in each condition (*centered*, *overlapped*, *adjacent* and *far*) and in each adaptation strength as we had done for the experimental data (Figure 8).

As shown in Figure 9, the model was able to reproduce the fact that the calcium and LFP signals were correlated independently of the brain state in all the conditions: 0.2 ± 0.03 Pearson's correlation and 0.53 ± 0.03 peak correlation on average (across conditions and brain states). Moreover, the model also showed a delay between the LFP and the calcium signal that decreased with the strength of adaptation in all conditions, with an average value of 0.13 ± 0.05 seconds. Importantly, for each brain state we observed that the delay increased with the distance between calcium and LFP regions, finding the largest delay in the *far* condition, in which the LFP and the calcium signals are computed from very distant populations of neurons. We found the same result averaging across the different adaptation strengths. Therefore, we conclude that the delay is due to the fact that the calcium and the LFP signals come from slightly different regions of the brain and that when the brain activity is more synchronous this delay is reduced without affecting the correlation value.

Up and Down states detection. An important feature for assessing the level of consciousness is the presence or absence of slow oscillations, and if present, the length of Up and Down states and the frequency of the slow oscillation^{12,37}.

These relevant measures depend on the accuracy of the detection of Up and Down states, usually performed on electrophysiological signals such as the LFP. Here we want to test the suitability of calcium signals for Up and Down states detection and therefore demonstrate that it is possible to assess the level of consciousness with calcium imaging techniques.

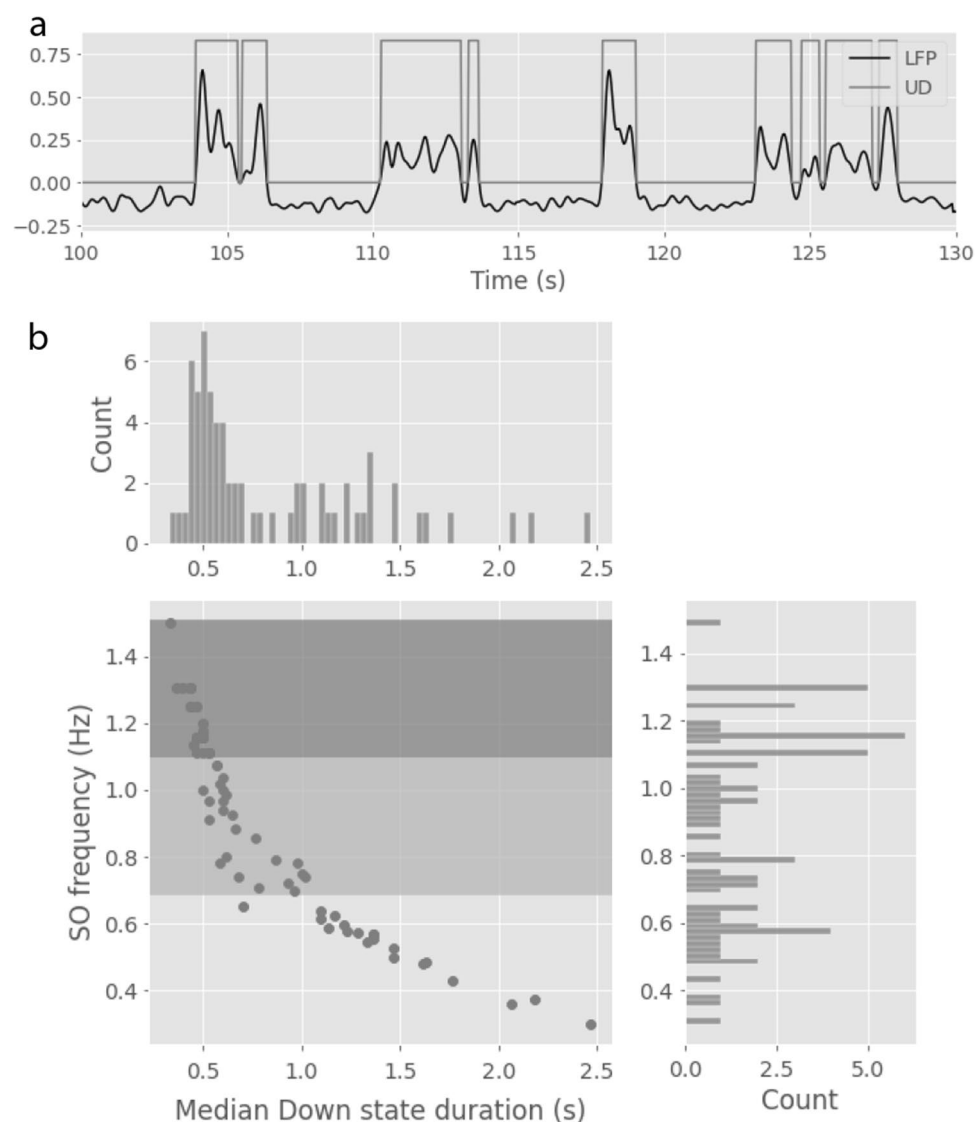


Figure 3. Up and Down state dynamics in the LFP. **a.** Example of Up and Down state detection in a 30 seconds recording using the normalized LFP signal (arbitrary units). **b.** Relationship between SO frequency and Down state duration across recordings. Definition of three groups of recordings of decreasing slow oscillation frequency. Data from 67 recordings (8 mice).

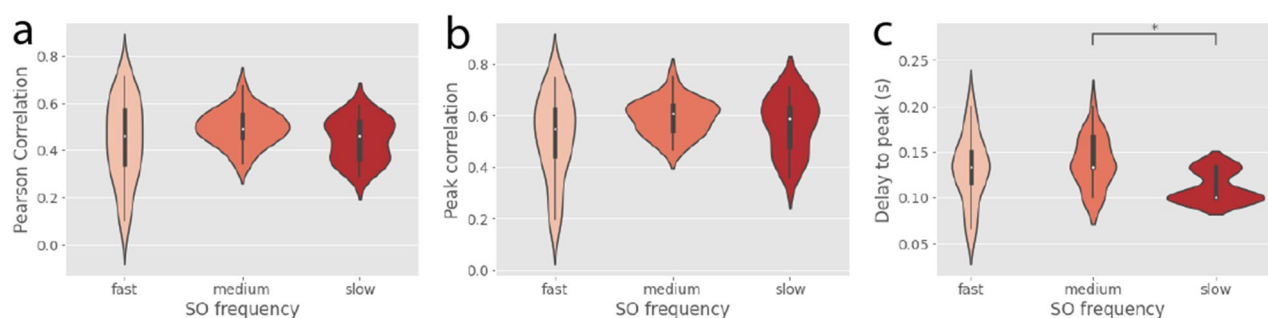


Figure 4. Correlation between LFP and calcium signals. LFP-FOV Pearson's correlation (**a**), peak cross-correlation (**b**) and delay to peak (**c**) as a function of slow oscillation frequency (n=67 recordings, 8 mice).

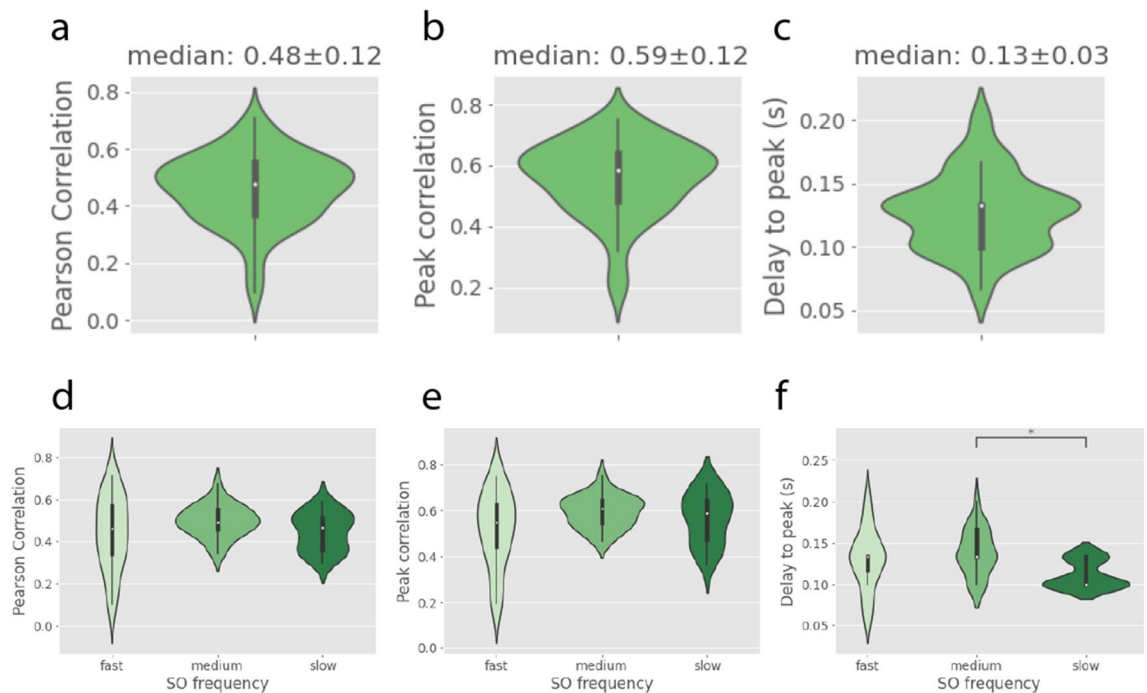


Figure 5. LFP-NPL correlation measures. a-c. Median values of the Pearson's correlation, Peak cross-correlation and Delay to the cross-correlation peak across $n=67$ recordings (8 mice). d-f. Same correlation measures plotted across different levels of anesthesia.

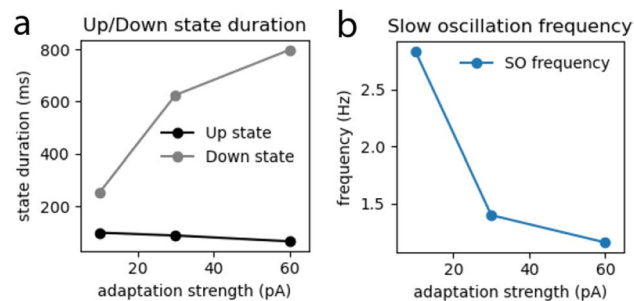


Figure 6. Slow oscillation measures at increasing adaptation strengths: Up and Down state duration (a) and frequency of the slow oscillation (b) at increasing adaptation strength (parameter b in the model).

We used the same algorithm (see Methods section) to detect Up and Down states from LFP and FOV signals in each recording (Figure 10).

We found that the median duration of Up or Down states, as well as the median frequency of the slow oscillation detected with either the LFP or the FOV signal are practically the same: 0.40 ± 0.12 s versus 0.37 ± 0.11 s for the median Up state duration; 0.60 ± 0.48 s versus 0.67 ± 0.36 s for the median Down state duration and 0.92 ± 0.29 Hz versus 0.91 ± 0.28 Hz for the median slow oscillation frequency, using the LFP or the FOV signals, respectively (Figure 11).

Discussion

In this paper, we have explored whether the calcium signals from two-photon (2P) calcium imaging can be used to assess brain state, in this case, the level of anesthesia. In particular, we focused on either the wide field signal (FOV) or the signal from the neuropil (NPL, removing somata from FOV). By measuring these signals simultaneously with a microelectrode for LFP recording, we found a high correlation between LFP and FOV/NPL. We further showed that this level of correlation did not change with the level of anesthesia, which is good evidence that the correlation is not due to network activity but stems from a real overlap between the two signals. However, we also found that the delay between the LFP and the two-photon signal (both FOV and NLP) was dependent on brain state, and was significantly smaller for deeper anesthesia. Using computational models, we could reproduce this result, predicting that the delay is due to the fact that the calcium and the LFP signals come from slightly different regions of the brain. When brain activity is more synchronous, this delay is reduced without affecting the correlation value. Thus, calcium signals appear to be suitable to assess brain state, and perform

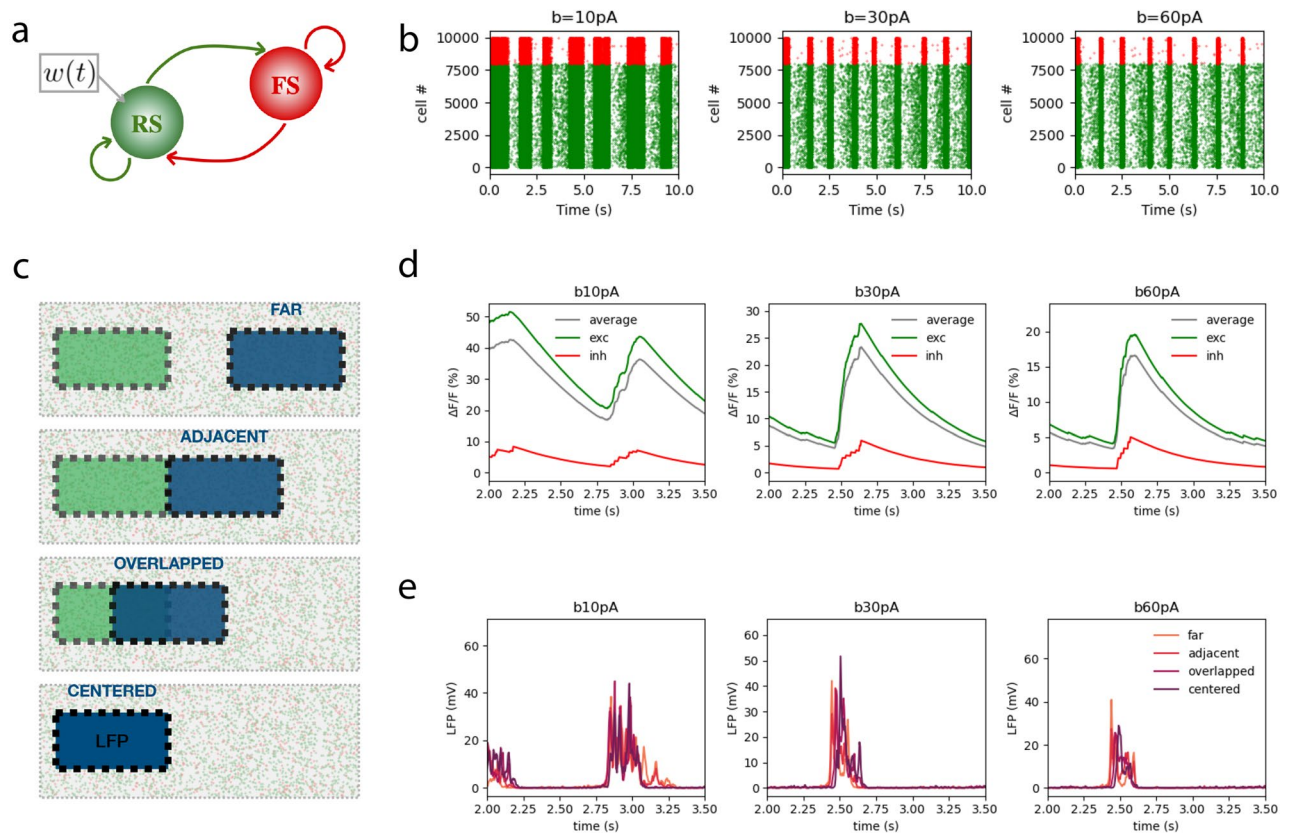


Figure 7. Simulations of calcium and LFP signals: **a.** The spiking network model has two populations: one of fast spiking (FS) inhibitory neurons and another of regular spiking (RS) excitatory neurons, which are affected by adaptation ($\omega(t)$). **b.** Raster plots of the spikes of each population (red for inhibitory cells and green for excitatory cells) simulated under increasing adaptation strength (from left to right the strength of adaptation is $b = 10, 30$ and 60 pA , respectively). **c.** 2D plane in which the 10k simulated neurons are located and position of the LFP area (blue) relative to the calcium area (FOV, green) in each condition (the distance between centers in the *centered*, *overlapped*, *adjacent* and *far* conditions are 0, 300, 600 and $900\mu\text{m}$, respectively). Dimensions of the total area: $1700 \times 600\mu\text{m}^2$; FOV and LFP areas: $600 \times 300\mu\text{m}^2$. **d.** Calcium signal of the excitatory (green), inhibitory (red) and average (grey) populations, simulated under increasing adaptation strength as in **b.** **e.** LFP signal in each condition in **c**, simulated under increasing adaptation strength as in **b.**

Up and Down states detection (which is difficult with 2P data from cellular spiking activity). In the following, we discuss the significance of these main findings, relate them to previous work, and outline perspectives that they offer for future work.

One of the very first study to combine LFP recordings with 2P calcium imaging was done by¹⁹ in an attempt to measure the “input” and “output” of neocortical networks *in vivo*. In that study, the authors reported that the neuropil signal, which they called “Optical Encephalogram” (OEG), is highly correlated with the surface potential, the electro-corticogram (ECoG). This is in full agreement with the measurements we provide here, where the LFP is found to be highly correlated to the neuropil signal generated by excitatory neurons. As the neuropil signal results from a combination of synaptic calcium signals in dendrites, action potentials in axons, and glia, the authors qualified the OEG as providing information about the “input” of the network. In the framework of assessing brain state, we suggest here that the calcium signal from excitatory neurons also provides a measurement of the distributed activity similar to the LFP, which is thought to be dominated by synaptic currents⁹.

It is important to note that it was found that LFP signals contain a strong contribution from inhibitory post-synaptic currents (IPSCs) in human and monkey³⁴. This conclusion was reached by calculating the relationship between the 96 LFP electrodes in Utah-array recordings, with single-unit activity of regular-spiking (RS) and fast-spiking (FS) neurons. FS cells produce the strongest unitary fields compared to RS cells, corroborating previous studies in hippocampal slices^{5,14}. Our measurements do not provide information about a possible dominance of IPSCs in LFP or neuropil activity, but we expect that IPSCs do contribute to the neuropil and FOV signals, as they participate to sculpt the voltage activity in dendrites. Thus, the correlation we find between LFP and field of view or neuropil signals could be due, in part, to the postsynaptic contribution of inhibitory neurons.

More recent work by⁷ also used 2P calcium imaging, to show that Layer 5 pyramidal neurons strongly synchronize during slow oscillations during anesthesia. The present recordings were done in superficial layers (essentially Layer 2/3), where we found that the neuropil and FOV signals correlate with the LFP oscillations during anesthesia. As the calcium signal was due to pyramidal cells in our preparation, the neuropil signal presumably contains contributions from all dendrites in superficial layers, which include Layer 2/3 pyramidal cell

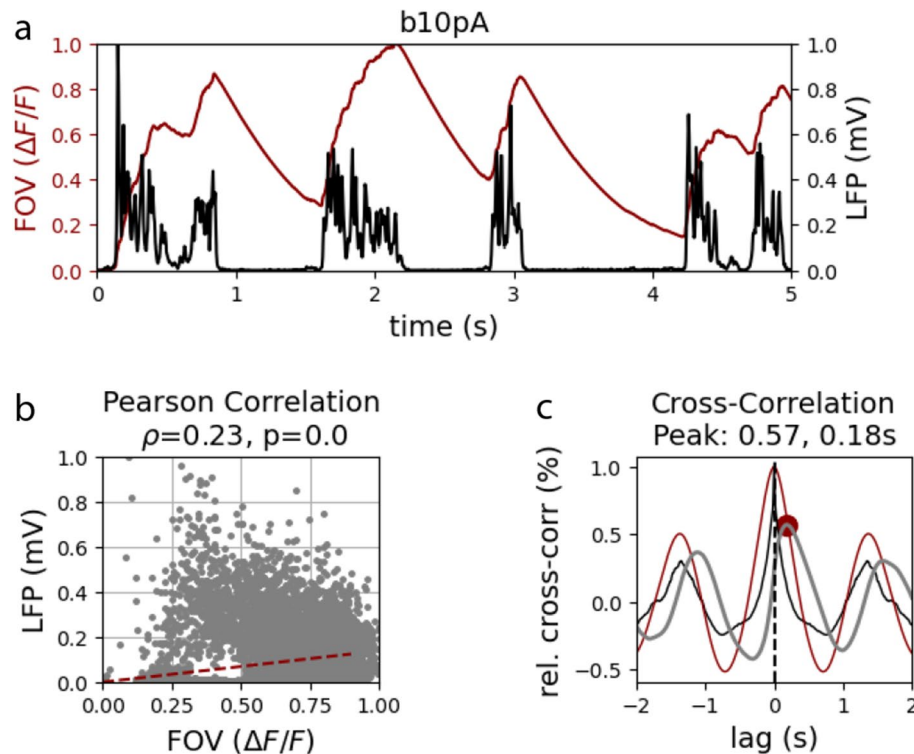


Figure 8. Correlation measures in the model. **a.** Simulated calcium and LFP normalized signals during 20 seconds of simulation at $b = 10\text{ pA}$ (light anesthesia) in the *centered* condition. **b.** Pearson's correlation. **c.** Auto- and cross-correlation of LFP (black trace) and calcium (red trace) signals. The cross-correlation (grey trace) peak is depicted with a red dot.

dendrites, but also deep layer pyramidal cell apical dendrites. Thus the correlations we find are also in agreement with this recent study.

One of our main findings is that the correlation between LFP and the calcium signal did not depend on brain state, which suggests that both the neuropil and FOV reflect information similar to the LFP, and thus can be used to infer the state of the brain similarly to the LFP.

However, we also found that there is a substantial delay between the two signals, which can be in 100 ms range. Even though calcium dynamics are used as a proxy for neuronal spiking activity, biophysical constraints make calcium dynamics significantly slower than membrane potential fluctuations^{3,32}. Indeed, ionic diffusion/extrusion and intrinsic and extrinsic calcium buffers result in complicated interactions that affect calcium kinetics²². Interestingly, the intrinsic delay between electrophysiological recordings and GCaMP6f signal has been reported to be ~ 40 ms both at single cell level¹⁰ and at the population level²⁰. Thus we considered this delay as a fixed component of the delay we observed. Despite this static component which is an intrinsic property of the calcium measure, here we found a brain-state dependent component of the delay.

We propose two different methods for evaluating the level of correspondence between electrophysiological and calcium imaging signals. On the one hand, we measure the cross-correlation peak between the signals, and the delay to this peak. On the other hand, we first detect Up and Down states and then measure some characteristic properties of the slow oscillation. Of course, the second method can only be used in the presence of slow oscillations, and in consequence, this methodology would not be indicated in the case of brain states in which the activity is desynchronized, such as quiet wakefulness, running, or some phases of natural sleep.

We provided a computational model to explain these results where we took into account the fact that the LFP electrode was located outside of the imaged field. The model predicts that the delay is due to this spatial separation, and that the state dependence of the delay can be accounted for by the different levels of synchrony of different brain states. But most importantly, the model could reproduce the state independence of the correlations between the calcium and LFP signals. In future work, it would be interesting to further check these model predictions by using more realistic models of the cortical tissue, where the various cellular processes (soma, dendrites, axons, glial cells) are explicitly integrated for a more quantitative match with the experimental measurements.

Recently, the development of transparent graphene microelectrode technology enabling crosstalk-free integration of 2P microscopy, optogenetics, and cortical recordings in vivo will represent a useful tool for dissecting the correlation of the electrical and optical signal over a larger spatial scale³⁶. Finally, a perspective would be to follow a similar approach at a larger scale, by relating signals such as the wide-field calcium signal, with large-scale electric signals such as the EcoG or the electro-encephalogram (EEG) (e.g. as in^{16,38}). The present observation that the field-of-view signal and neuropil signal largely overlap, shows that the contribution of somata

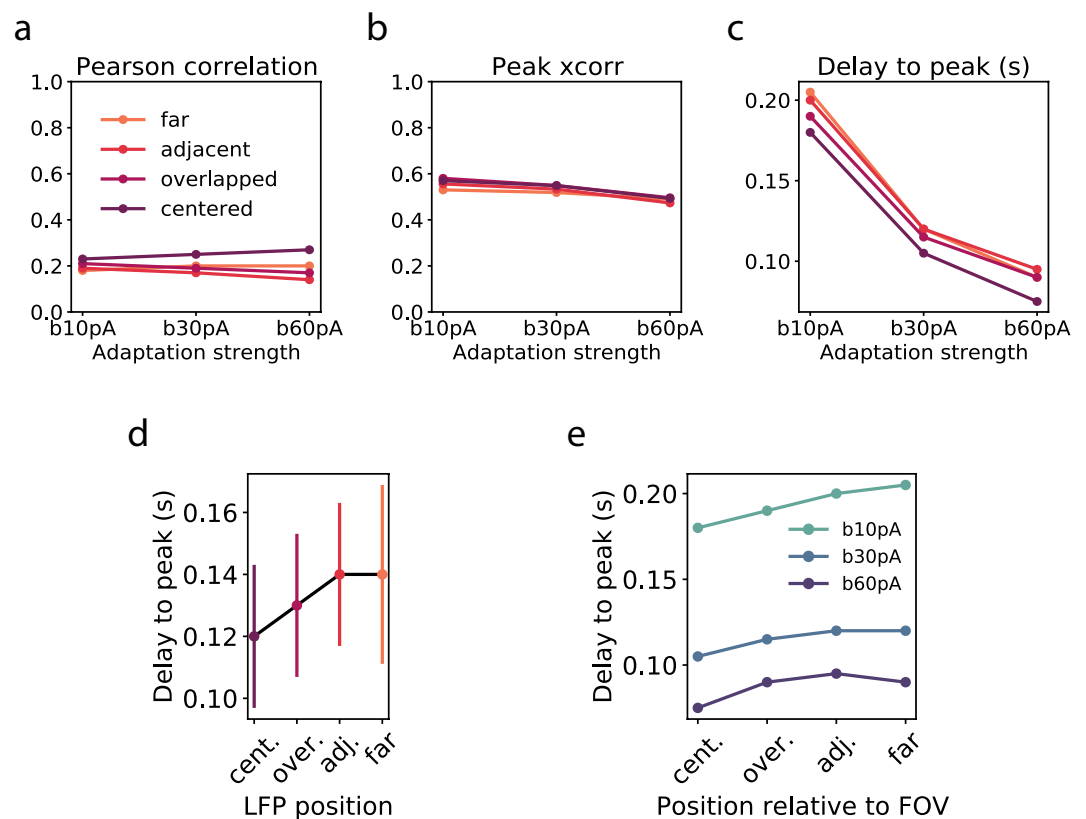


Figure 9. Correlation between calcium and LFP for each condition. a-c. Pearson's correlation, peak cross-correlation and delay to peak as a function of the adaptation strength. Colors indicate the condition, that is the position of the LFP area with respect to the calcium area. **d.** Average across different adaptation strengths of the delay to peak as a function of the condition. Error bars indicate the standard error of the mean. **e.** In each adaptation strength, delay to peak as a function of the condition.

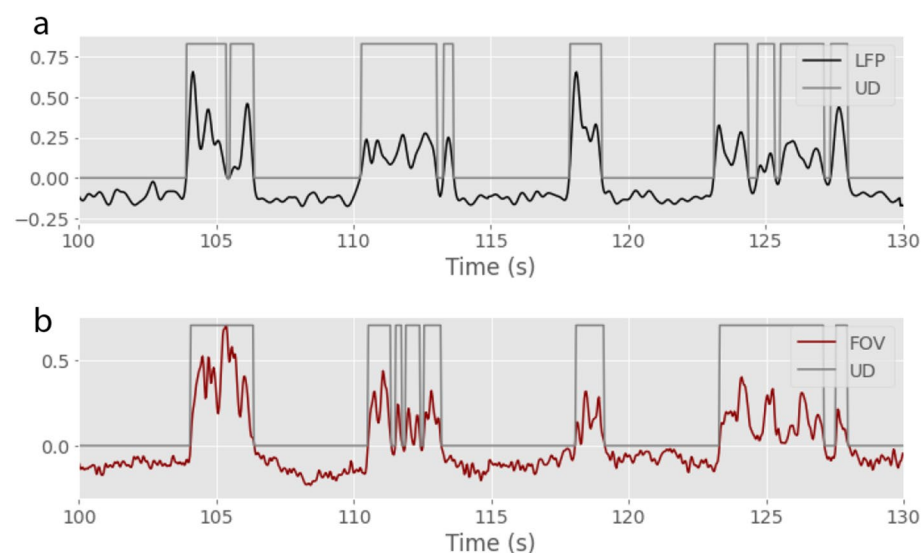


Figure 10. Up and Down state detection in LFP and calcium signals. Example of Up and Down state detection in a 30 seconds recording using the LFP (a) or the FOV (b) signals. .

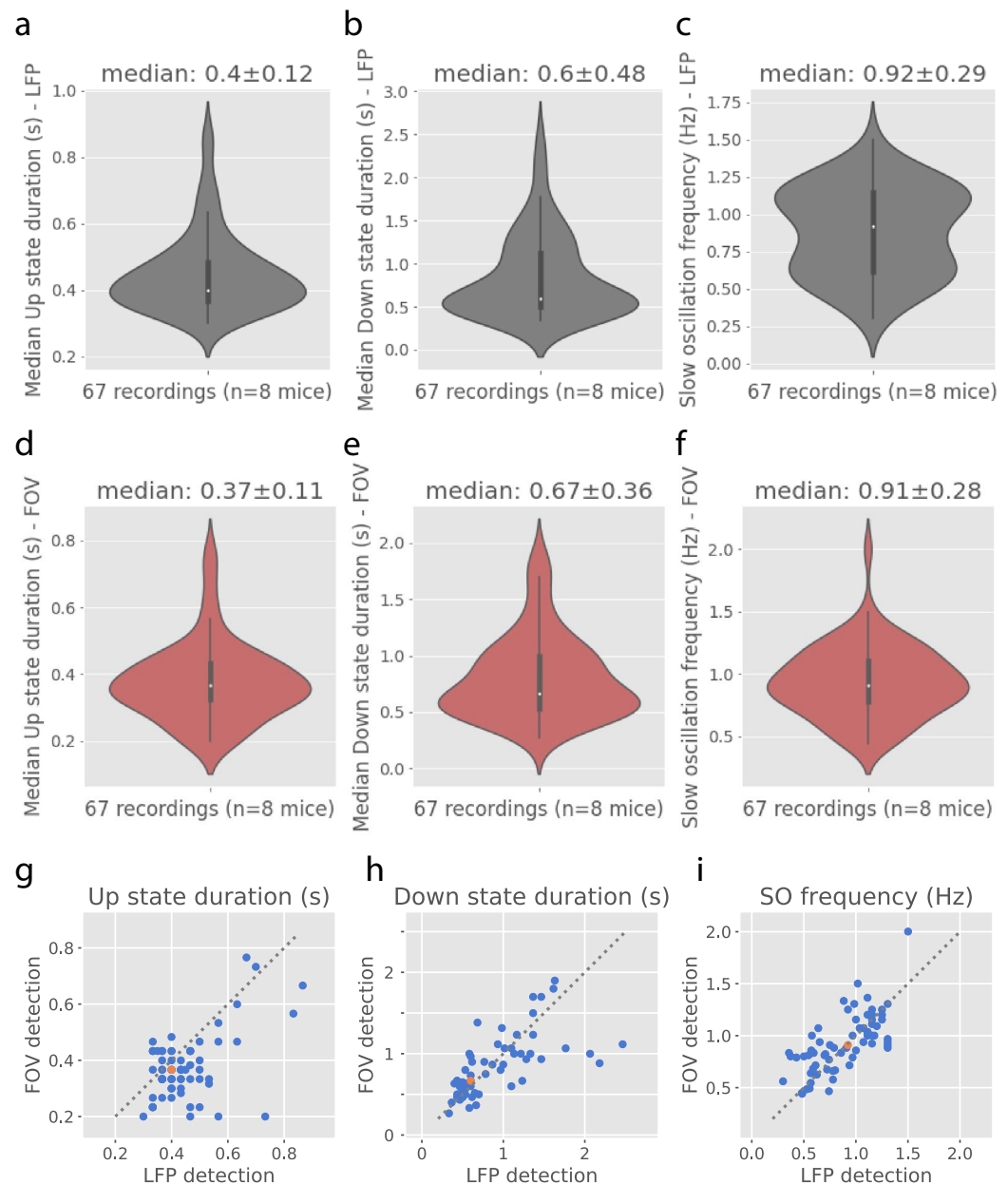


Figure 11. Up and Down state detection from FOV or LFP signals From left to right, Up state duration, Down state duration and frequency of the slow oscillation detected with the LFP signal (a-c.) or the FOV signal (d-f.). g-i. Correspondence between LFP and FOV measures shown graphically. Each blue dot corresponds to a different recording. The orange dot is the median. The grey dashed line is the model $x=y$.

is comparatively small. A consequence is that wide-field calcium signals measured from the brain surface, are perhaps also dominated by synaptic currents and should thus highly correlate with EcoG or EEG signals. This should be examined by future studies where these signals could be recorded simultaneously. Last, extending the present study on slow-wave activity to other physiological states like running, resting, and natural sleep, will be necessary to understand possible changes in the correlation of the calcium and LFP signals in awake subjects.

Materials and methods

Experimental recordings. All experimental procedures were performed in accordance with the ARRIVE guidelines (<https://arriveguidelines.org>), the directive 2010/63/EU on the protection of animals used for scientific purposes and approved by the Italian Minister of Health, authorization n. 723/2019. We recorded the cortical activity from $n = 8$ Thy1-GCaMP6f mice (RRID:IMSR_JAX:025393¹¹); 4 females and 4 males with average weights 35 ± 3 g and 40 ± 4 g, respectively.

For the surgery, mice were deeply anesthetized with isoflurane. The protocol followed for the cranial window preparation was slightly modified from¹⁷ and²¹. Briefly, we administered anesthetized mice a subcutaneous injection of dexamethasone (0.04 mL per 2 mg/mL). The animals were then placed into a stereotaxic apparatus and after applying the local anesthetic lidocaine 2% (20 mg/mL), the skin over the skull was removed. Using a dental drill, the border of a 3-mm-wide circular area above the primary somatosensory cortex (AP -2 mm, ML +2 mm from bregma) was thinned and the central part of the bone was gently removed. The exposed brain was covered with a cover glass, leaving a small portion of the window open for the LFP electrode to be inserted. The optical window was sealed to the skull with a mixture of dental cement and acrylic glue. The exposed skull was covered using dental cement (Super Bond, C & S, Sun medical Moriyama City, Shiga, Japan). The surgery was followed by the imaging session under the two-photon microscope. To induce different brain states we used different doses of isoflurane anesthesia. The commercial apparatus for two-photon microscopy (Bergamo II Series Multiphoton Microscope, Thorlabs) was combined with a mode-locked Ti: Sapphire laser (Chameleon, Coherent Inc.) to supply the excitation light. The laser beam was scanned in the xy plane by a galvo-resonant system. An objective lens (XLUM 20X, NA 0.95, WD 2 mm, Olympus) focused the beam onto the specimen. A closed-loop piezoelectric stage allowed axial displacements of the objective.

To record the LFP signals, we inserted a pipette filled with 1mM Rhodamine dye at the edge of the imaging area. LFP was recorded using a borosilicate glass microelectrode (8–10 M Ω), backfilled with a filtered solution of 2M NaCl and 0.1mM sulforhodamine 101 (S76352, Sigma-Aldrich) to allow the electrode tip visualization. The microelectrode was placed under visual guidance into the cortical layer 2/3, coplanar with the imaging depth. A reference screw was placed on the contralateral parietal bone and a ground screw was placed on the occipital bone.

Voltage signals were recorded using a 3000 AC/DC differential amplifier, sampled at 10 kHz, high-pass filtered at 0.1 Hz, low-pass filtered at 3 kHz and digitized at 10 kHz using a USB-621 interface (National Instruments).

After the imaging session, all animals were perfused with 150 mL of paraformaldehyde 4% (PFA, Aldrich, St. Louis, Missouri, USA).

Signal synchronization. A file containing the triggers for the calcium recordings (signalling the onset of each two-photon scan) was sampled at the same sampling frequency as the LFP signal (10 kHz). Using these triggers we aligned the LFP and calcium signals, and downsampled the LFP at the same sampling rate as the two-photon signals (30 Hz), by averaging the LFP signal between two consecutive two-photon samples.

Neuropil computation. To compute the neuropil (NPL) signal from the calcium signals in each recording, the somas of the cells were identified, and the average activity of the pixels corresponding to the soma area was saved independently for each cell. Then, the activity of all the cells was subtracted from the Field of View (FOV) signal, that is the average signal from all the pixels (1025x512 pixels).

Signal processing. The signals were processed to filter out the low frequency components responsible of the drifts, and the higher frequency components that correspond to noise. The LFP signal was filtered between 10 and 15 Hz. This resulted in a LFP signal that increased with increased activity, independently of the depth of the tip of the electrode. FOV and NPL signals, on the contrary, had more noise in this frequency range, so we filtered them between 0.1 and 1.5 Hz. All signals were normalized after filtering.

Correlation measures. To compare the LFP signals with the calcium signals we used Pearson's correlation and cross-correlation. We normalized the cross-correlation values by the standard deviation of the two signals. We evaluated the *peak correlation* as the normalized cross-correlation value at the peak and the *zero-lag correlation* as the normalized cross-correlation value at the zero lag which corresponded to the Pearson's correlation value (not shown). The *delay to peak* was evaluated as the lag at which the cross-correlation peaked.

Statistics. To compare the different levels of anesthesia we used ANOVA and Tukey's method for post-hoc testing the significance of the differences between pairs of groups. All the analyses were performed using the module statsmodels in python scripts.

Up and Down state detection. The normalized signal was sliced in smaller chunks of 15 seconds. For each chunk, the mean was subtracted and the standard deviation (STD) computed. Then a threshold was set at 0.1 times this STD. Periods longer than 80 ms in this 15 second signal that were over the threshold were marked as an Up state.

Spiking network model. The network contains $N = 10,000$ neurons. 20% of them are inhibitory, fast spiking neurons and the other 80% are excitatory, regular spiking neurons. The neurons are modeled as adaptive exponential integrate and fire (*Adex*) neurons⁸. Including spike frequency adaptation, a network of *Adex* neurons can reproduce both asynchronous or synchronous activity regimes¹³, and therefore is ideal to simulate the cortical dynamics of different levels of consciousness or brain states such as wakefulness, sleep or anesthesia^{2,23}. The equations that drive the dynamics of *Adex* neurons are the following:

$$C_m \frac{dV}{dt} = -G_l(V - E_l) + G_l \Delta_V \exp\left(\frac{V - V_{thre}}{\Delta_V}\right) + I_{syn} + \sigma \xi - \omega$$

$$\frac{d\omega}{dt} = -\frac{\omega}{\tau_\omega} + b \sum_k \delta(t - t_k) + a(V - E_l)$$

where the synaptic input is defined as:

$$I_{syn} = \sum_i g_i^{syn} (V - E_i^{syn}) \quad (1)$$

with

$$\frac{dg_i^{syn}}{dt} = -g_i^{syn} / \tau_{syn} \quad (2)$$

As in², the leak conductance is $G_l = 10nS$, the membrane capacitance is $C_m = 150pF$, the resting potential is $E_l = -60mV$ for excitatory cells and $E_l = -65mV$ for inhibitory cells, the steepness of the exponential approach to threshold is $\Delta_V = 2.0$ and $\Delta_V = 0.5$ for excitatory and inhibitory cells, respectively, the spiking threshold is $V_{thre} = -50mV$, the refractory period is defined by $V_{reset} = -60mV$ and $T_{refrac} = 5ms$. The term $\sigma \xi$ in the membrane potential equation represents a gaussian noise of amplitude $\sigma = 50$. The adaptation ω is modeled with the parameters $a = 4nS$ and $\tau_\omega = 500ms$. To simulate increasing levels of isoflurane anesthesia we used different values of the parameter b in the model, that represents the strength of adaptation: at each spike, the adaptation current is incremented by a value b .

Gaussian connectivity. The neurons are connected following a distance-dependent rule and a certain probability of connection that depends on the type of synapse:

$$p_{ij} = p_0 \exp\left(-\frac{(x_i - x_j)^2 + (y_i - y_j)^2}{2\sigma^2}\right) \quad (3)$$

where $p_0 = 0.205$, $\sigma = 130\mu m$ for excitatory synapses and $p_0 = 0.72$, $\sigma = 110\mu m$ for inhibitory synapses.

Calcium model. We used the calcium model described in², where we take into account the dynamics of voltage gated calcium channels to translate the changes in the membrane potential due to the spiking activity into inward current of calcium ions. Then we evaluate the internal concentration of calcium as a function of these currents and the slow decay to the basal concentration of calcium ($\tau_{Ca} = 760ms$). Finally, we compute the calcium signal (fluorescence) as a function of the internal calcium concentration taking into account the specific calcium indicator (GCaMP6f) parameters:

$$Ca = k_F \frac{[Ca^{2+}]^{n_H}}{[Ca^{2+}]^{n_H} + k_d} \quad (4)$$

where $K_F = 10$ is a scaling factor, $k_d = 375nM$ is the dissociation time constant for GCaMP6f, a measure of the affinity of the fluorescent indicator to the calcium ion, and $n_H = 2.3$ is the Hill coefficient¹⁰.

The calcium signal was obtained for the excitatory and inhibitory populations (Ca_{exc} and Ca_{inh} , respectively). The average calcium signal (Ca) of the network was computed as follows:

$$Ca = 0.2 * Ca_{inh} + 0.8 * Ca_{exc} \quad (5)$$

LFP model. To estimate the LFP from the spiking neurons we use the method described in³⁵. We consider the LFP recorded in the center of a squared area of $600 \times 300\mu m$. The LFP generated by each population is computed as the sum of the unitary LFPs ($uLFP$) obtained from the convolution of the spike train of each neuron with a gaussian kernel:

$$uLFP(x, t) = A(x) \exp\left(-\frac{(t - tp)^2}{2\sigma^2}\right) \quad (6)$$

where $A(x)$ is an amplitude that decays with the distance:

$$A(x) = A_0 \exp\left(-\frac{|x - x_0|}{\lambda}\right), \quad (7)$$

with the maximal amplitude $A_0 = 3\mu V$ and $0.48\mu V$ for the inhibitory and the excitatory cells, respectively, as we consider the LFP recorded from the *soma* layer, and the space constant of the decay $\lambda = 0.2mm$. $|x - x_0|$ is the distance between the position of the electrode and the soma of each cell.

σ in equation 6 is the standard deviation in time and takes the values 2.1 and 3.15ms, for inhibitory and excitatory cells, respectively, and tp is the peak time of the $uLFP$, defined as:

$$t = t_0 + d + |x - x_0|/v_a, \quad (8)$$

where t_0 is the time of the spike, $d = 10.4ms$ is a constant delay and the axonal velocity is $v_a = 0.2m/s$.

The average LFP over populations was computed as:

$$LFP = 0.2 * LFP_{inh} + 0.8 * LFP_{exc} \quad (9)$$

Data availability

The datasets used and/or analysed during the current study available from the corresponding author on reasonable request.

Received: 7 December 2022; Accepted: 17 February 2023

Published online: 23 February 2023

References

1. Aedo-Jury, F., Schwalm, M., Hamzehpour, L. & Stroh, A. Brain states govern the spatio-temporal dynamics of resting-state functional connectivity. *eLife* **9**, e53186 (2020).
2. Allegra Mascaro, A. L. *et al.* Experimental and computational study on motor control and recovery after stroke: Toward a constructive loop between experimental and virtual embodied neuroscience. *Front. Syst. Neurosci.* **14**, 31 (2020).
3. Bando, Y., Sakamoto, M., Kim, S., Ayzenshtat, I. & Yuste, R. Comparative evaluation of genetically encoded voltage indicators. *Cell Rep.* **26**(3), 802–813 (2019).
4. Bando, Y., Wenzel, M. & Yuste, R. Simultaneous two-photon imaging of action potentials and subthreshold inputs in vivo. *Nat. Commun.* **12**(1), 7229 (2021).
5. Bazelot, M., Dinocourt, C., Cohen, I. & Miles, R. Unitary inhibitory field potentials in the CA3 region of rat hippocampus. *J. Physiol.* **588**(Pt 12), 2077–90 (2010).
6. Bettinardi, R. G., Tort-Colet, N., Ruiz-Mejias, M., Sanchez-Vives, M. V. & Deco, G. Gradual emergence of spontaneous correlated brain activity during fading of general anesthesia in rats: Evidences from fmri and local field potentials. *Neuroimage* **114**, 185–198 (2015).
7. Bharioke, A. *et al.* General anesthesia globally synchronizes activity selectively in layer 5 cortical pyramidal neurons. *Neuron* **110**, 2024–2040 (2022).
8. Brette, R. & Gerstner, W. Adaptive exponential integrate-and-fire model as an effective description of neuronal activity. *J. Neurophysiol.* **94**(5), 3637–3642 (2005).
9. Buzsáki, G., Anastassiou, C. A. & Koch, C. The origin of extracellular fields and currents-eeg, ecog, lfp and spikes. *Nat. Rev. Neurosci.* **13**(6), 407–420 (2012).
10. Chen, T.-W. *et al.* Ultrasensitive fluorescent proteins for imaging neuronal activity. *Nature* **499**(7458), 295–300 (2013).
11. Dana, H. *et al.* Thy1-gcamp6 transgenic mice for neuronal population imaging in vivo. *PLoS ONE* **9**(9), e108697 (2014).
12. Dasilva, M. *et al.* Modulation of cortical slow oscillations and complexity across anesthesia levels. *NeuroImage* **224**, 117415 (2021).
13. Destexhe, A. Self-sustained asynchronous irregular states and up-down states in thalamic, cortical and thalamocortical networks of nonlinear integrate-and-fire neurons. *J. Comput. Neurosci.* **27**(3), 493–506 (2009).
14. Glickfeld, L. L., Roberts, J. D., Somogyi, P. & Scanziani, M. Interneurons hyperpolarize pyramidal cells along their entire somatodendritic axis. *Nat. Neurosci.* **12**(1), 21–3 (2009).
15. Golshani, P. *et al.* Internally mediated developmental desynchronization of neocortical network activity. *J. Neurosci.* **29**(35), 10890–10899 (2009).
16. Gui, S. *et al.* Revealing the cortical glutamatergic neural activity during burst suppression by simultaneous wide field calcium imaging and electroencephalography in mice. *Neuroscience* **469**, 110–124 (2021).
17. Holtmaat, A. *et al.* Long-term, high-resolution imaging in the mouse neocortex through a chronic cranial window. *Nat. Protoc.* **4**(8), 1128–1144 (2009).
18. Inoue, M. Genetically encoded calcium indicators to probe complex brain circuit dynamics in vivo. *Neurosci. Res.* **169**, 2–8 (2021).
19. Kerr, J. N., Greenberg, D. & Helmchen, F. Imaging input and output of neocortical networks in vivo. *Proc. Nat. Acad. Sci.* **102**(39), 14063–14068 (2005).
20. Li, P. *et al.* Measuring sharp waves and oscillatory population activity with the genetically encoded calcium indicator gcamp6f. *Front. Cell. Neurosci.* **13**, 274 (2019).
21. Mascaro, A. L. A. *et al.* Combined rehabilitation promotes the recovery of structural and functional features of healthy neuronal networks after stroke. *Cell Rep.* **28**(13), 3474–3485 (2019).
22. Neher, E. Usefulness and limitations of linear approximations to the understanding of Ca^{++} signals. *Cell Calcium* **24**(5–6), 345–357 (1998).
23. Nghiem, T.-A.E. *et al.* Cholinergic switch between two types of slow waves in cerebral cortex. *Cereb. Cortex* **30**(6), 3451–3466 (2020).
24. Niethard, N., Brodt, S. & Born, J. Cell-type-specific dynamics of calcium activity in cortical circuits over the course of slow-wave sleep and rapid eye movement sleep. *J. Neurosci.* **41**(19), 4212–4222 (2021).
25. Niethard, N. *et al.* Sleep-stage-specific regulation of cortical excitation and inhibition. *Curr. Biol.* **26**(20), 2739–2749 (2016).
26. Niethard, N., Ngo, H.-V.V., Ehrlich, I. & Born, J. Cortical circuit activity underlying sleep slow oscillations and spindles. *Proc. Nat. Acad. Sci.* **115**(39), E9220–E9229 (2018).
27. Rochefort, N. L. *et al.* Sparsification of neuronal activity in the visual cortex at eye-opening. *Proc. Nat. Acad. Sci.* **106**(35), 15049–15054 (2009).
28. Sancataldo, G., Silvestri, L., Mascaro, A. L. A., Sacconi, L. & Pavone, F. S. Advanced fluorescence microscopy for in vivo imaging of neuronal activity. *Optica* **6**(6), 758–765 (2019).
29. Schwalm, M. *et al.* Cortex-wide bold fmri activity reflects locally-recorded slow oscillation-associated calcium waves. *eLife* **6**, e27602 (2017).
30. Shen, Y., Nasu, Y., Shkolnikov, I., Kim, A. & Campbell, R. E. Engineering genetically encoded fluorescent indicators for imaging of neuronal activity: Progress and prospects. *Neurosci. Res.* **152**, 3–14 (2020).
31. Shew, W. L., Bellay, T. & Plenz, D. Simultaneous multi-electrode array recording and two-photon calcium imaging of neural activity. *J. Neurosci. Methods* **192**(1), 75–82 (2010).
32. Smetters, D., Majewska, A. & Yuste, R. Detecting action potentials in neuronal populations with calcium imaging. *Methods* **18**(2), 215–221 (1999).
33. Stroh, A. *et al.* Making waves: Initiation and propagation of corticothalamic Ca^{2+} waves in vivo. *Neuron* **77**(6), 1136–1150 (2013).
34. Telenczuk, B. *et al.* Local field potentials primarily reflect inhibitory neuron activity in human and monkey cortex. *Sci. Rep.* **7**(1), 1–10 (2017).
35. Telenczuk, B., Telenczuk, M. & Destexhe, A. A kernel-based method to calculate local field potentials from networks of spiking neurons. *J. Neurosci. Methods* **344**, 108871 (2020).

36. Thunemann, M. *et al.* Deep 2-photon imaging and artifact-free optogenetics through transparent graphene microelectrode arrays. *Nat. Commun.* **9**(1), 2035 (2018).
37. Tort-Colet, N., Capone, C., Sanchez-Vives, M. V. & Mattia, M. Attractor competition enriches cortical dynamics during awakening from anesthesia. *Cell Rep.* **35**(12), 109270 (2021).
38. Wang, Z. *et al.* Rem sleep is associated with distinct global cortical dynamics and controlled by occipital cortex. *Nat. Commun.* **13**(1), 6896 (2022).
39. Wei, Z. *et al.* A comparison of neuronal population dynamics measured with calcium imaging and electrophysiology. *PLoS Comput. Biol.* **16**(9), e1008198 (2020).
40. Yang, W. *et al.* Anesthetics fragment hippocampal network activity, alter spine dynamics, and affect memory consolidation. *PLoS Biol.* **19**(4), e3001146 (2021).

Acknowledgements

This work has been funded by the CNRS and the European Community (Human Brain Project, H2020-785907 and H2020-945539).

Author contributions

NTC, FSP, LA, AD conceived the study; LA, EM and FR did the experiments and analyzed experimental data; NTC participated to the analysis and realized the computational model; all authors discussed the results and participated to write the paper; LA and AD co-supervised the study.

Competing interests

The authors declare no competing interests.

Additional information

Correspondence and requests for materials should be addressed to N.T.-C. or A.D.

Reprints and permissions information is available at www.nature.com/reprints.

Publisher's note Springer Nature remains neutral with regard to jurisdictional claims in published maps and institutional affiliations.



Open Access This article is licensed under a Creative Commons Attribution 4.0 International License, which permits use, sharing, adaptation, distribution and reproduction in any medium or format, as long as you give appropriate credit to the original author(s) and the source, provide a link to the Creative Commons licence, and indicate if changes were made. The images or other third party material in this article are included in the article's Creative Commons licence, unless indicated otherwise in a credit line to the material. If material is not included in the article's Creative Commons licence and your intended use is not permitted by statutory regulation or exceeds the permitted use, you will need to obtain permission directly from the copyright holder. To view a copy of this licence, visit <http://creativecommons.org/licenses/by/4.0/>.

© The Author(s) 2023